Electronic Supplementary Material (ESI) for RSC Advances.

Supporting Information

Highly dispersed ruthenium nanoparticles on nitrogen doped carbon toward efficient hydrogen evolution in both alkaline and acidic electrolytes

Gen Li[a], Rui Gao[a], Zhongyu Qiu[a], Wei Liu[a] and Yujiang Song[*a]

[a.] State Key Laboratory of Fine Chemicals, School of Chemical Engineering, Dalian University of Technology, 2 Linggong Road, Dalian 116024, China.

Corresponding author

* E-mail: yjsong@dlut.edu.cn

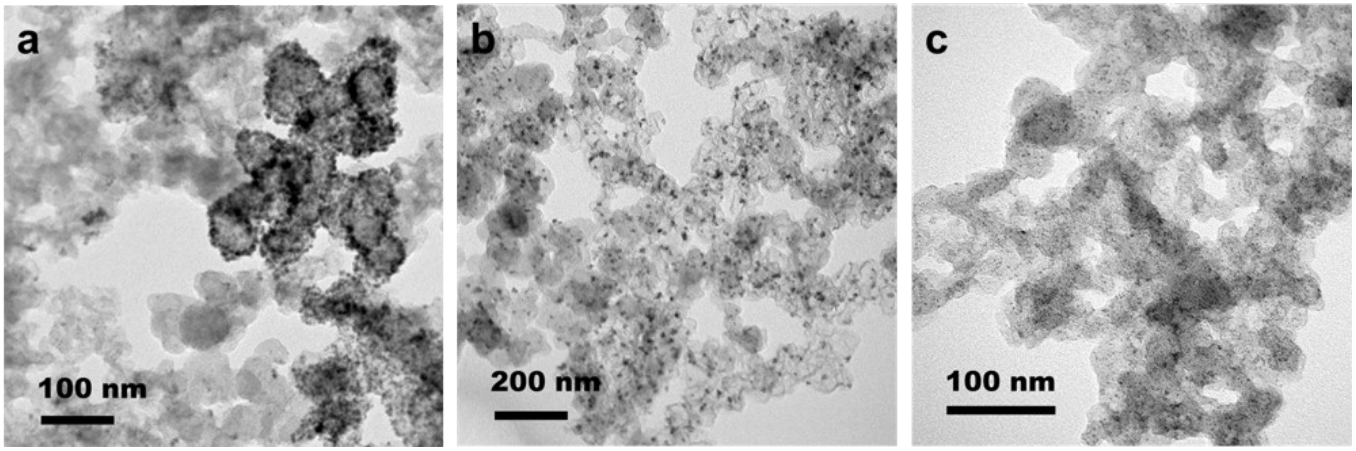

Fig. S1 TEM images of samples: (a) Carbon supported Ru NPs synthesized with sodium borohydride as reducing agent in water (Ru/C-$NaBH_4$); (b) Carbon supported Ru NPs synthesized with EG as reducing agent in EG (Ru/C-EG); (c) Carbon supported Ru NPs synthesized with EG as reducing agent in the presence of PVP as capping agent (PVP-Ru/C).

Fig. S1 give the understanding of the origin of highly dispersed ultrafine Ru NPs. EG has an appropriate reducing capacity and can well disperse EC600. Compared with Ru/C-$NaBH_4$, the particles of Ru/C-EG have significantly improved the distribution (Fig. S1 a, b). This results show that EG as a reducing agent can effectively promote the dispersion of Ru particles on the carrier. In addition, PVP, as a nitrogen-containing capping agent, can cover the surface of nanocrystalline during nucleation and growth process, and plays an important role in the formation of the nanocrystalline[1]. Thus, the introduction of PVP in EG system significantly inhibits the agglomeration of Ru, and ultrafine Ru nanoparticles were obtained while maintaining a highly dispersed state (Fig. S1 c).

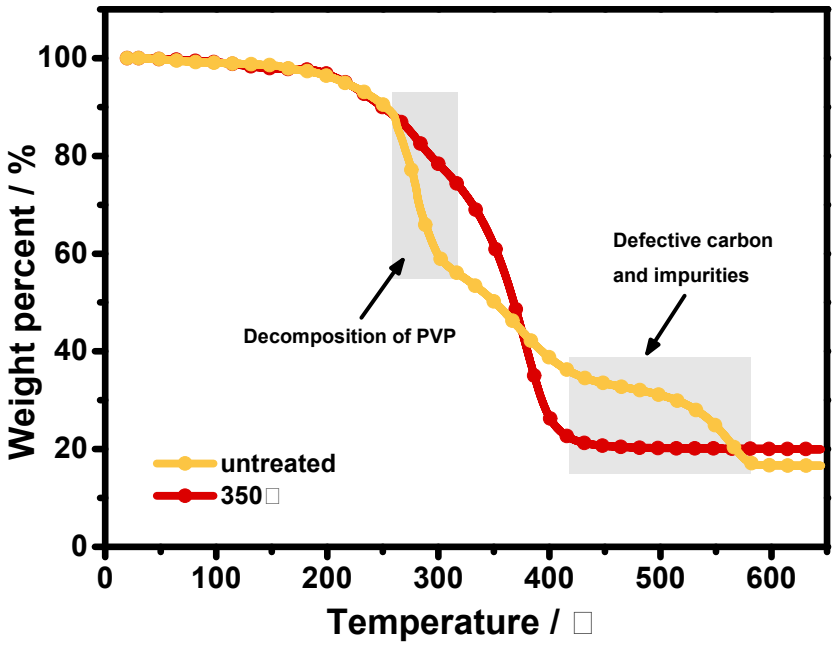

Fig. S2 TGA of carbon loaded Ru with adsorbed PVP before and after pyrolysis.

The N element of Ru/N-C comes from the pyrolysis of PVP. There exists an obvious weight loss stage from 250 to 350°C representing the thermal decomposition of adsorbed PVP. The weight loss between 420~550°C can be ascribed to the loss of amorphous carbon and impurities. After pyrolysis at 350°C, these two weight loss segments disappeared, indicating that adsorbed PVP has been well pyrolyzed.

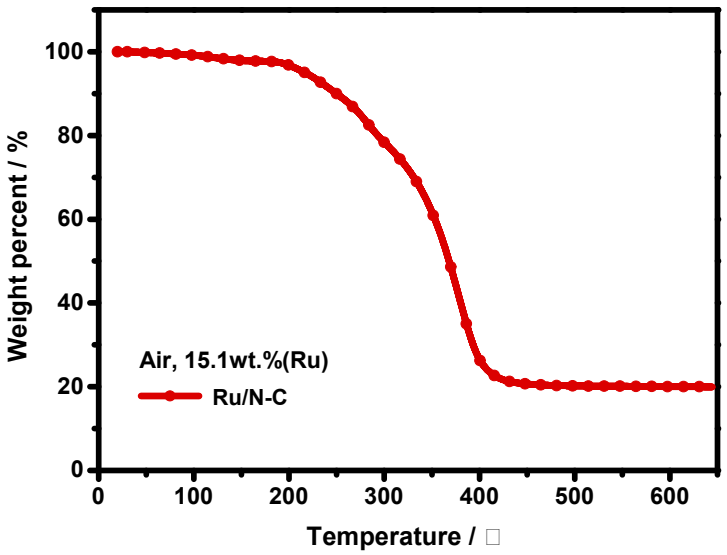

Fig. S3 TGA curve of Ru/N-C recorded in dry air with a heating rate of 10°C min^{-1}

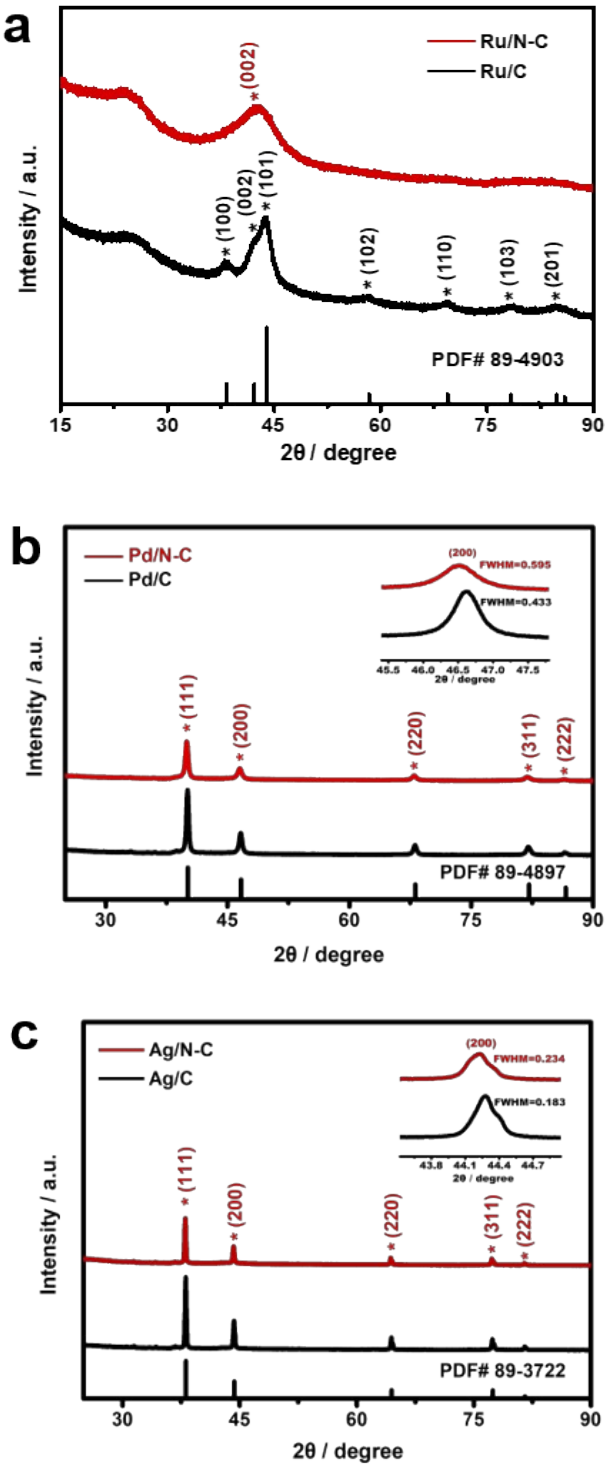

Fig. S4 (a) XRD patterns of Ru/N-C and Ru/C; (b) XRD patterns of Ag/N-C and Ag/C; (c) XRD patterns of Ag/N-C and Ag/C. Insets: enlarged (002) of Pd/C, Pd/N-C, Ag/C, and Ag/N-C.

Pd and Ag have faster reaction kinetics and different nucleation and growth habits from Ru, and it is more difficult to control the size. According to full width at half maximum (FWHM) before and after nitrogen doping, the particle size of Pd/N-C and Ag/N-C has also become smaller. This indicates that the synthetic strategy is general for particle size control.

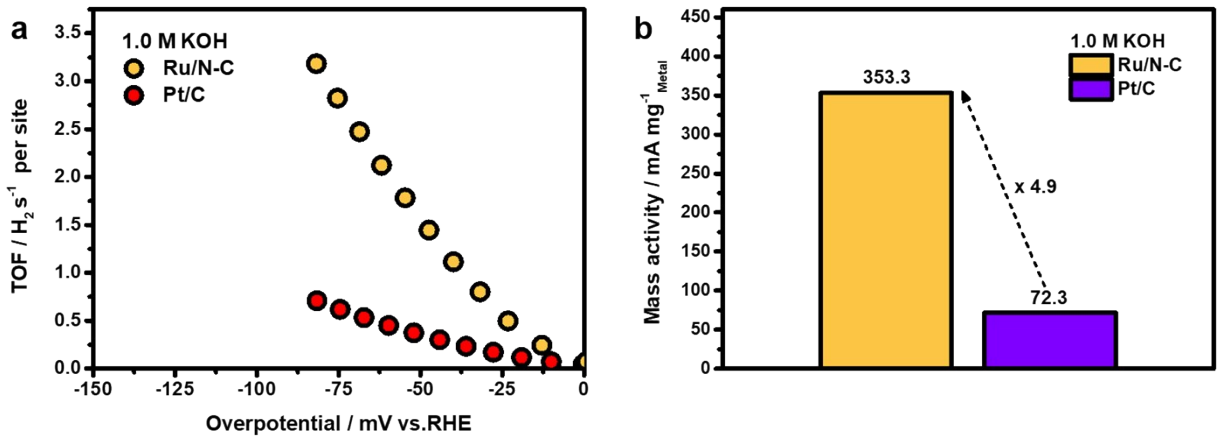

Fig. S5 (a) TOF of Ru/N-C and commercial Pt/C; (b) Mass activity of Ru/N-C and commercial Pt/C at the overpotential of 10 mV in N_2-saturated 1.0 M KOH aqueous solution.

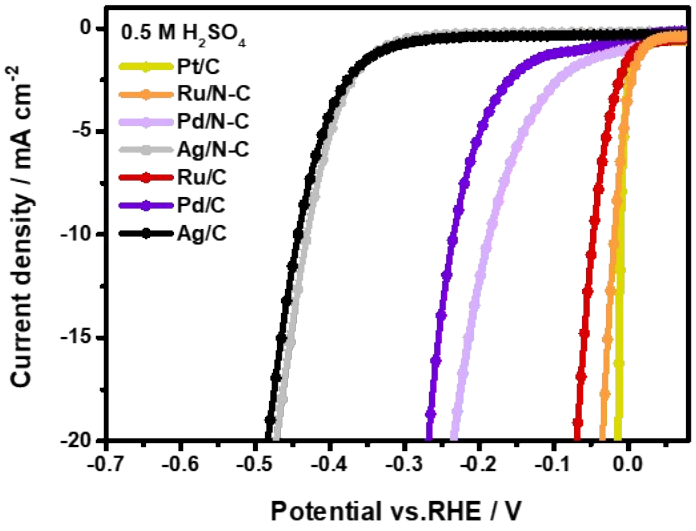

Fig. S6 Polarization curves of the electrocatalysts recorded in N_2-saturated 0.5 M H_2SO_4 aqueous solution with a scan rate of 5 mV s^{-1}.

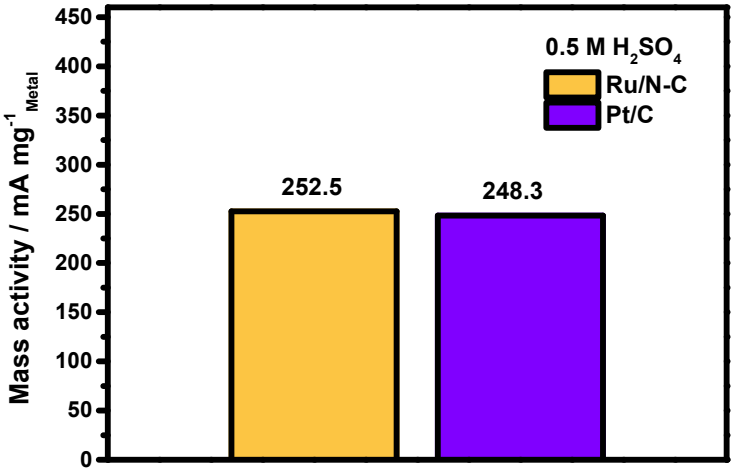

Fig. S7 Mass activity of Ru/N-C and Pt/C at the overpotential of 10 mV in N_2-saturated 0.5 M H_2SO_4 aqueous solution.

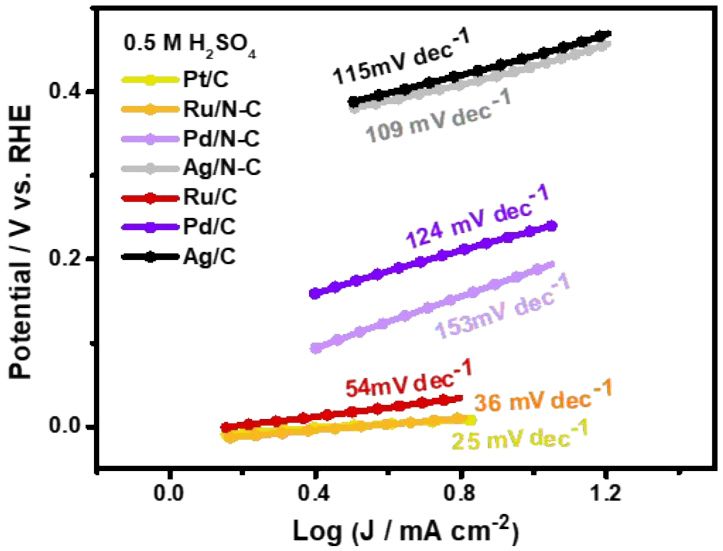

Fig. S8 Tafel plots of the electrocatalysts collected in N_2-saturated 0.5 M aqueous H_2SO_4 solution.

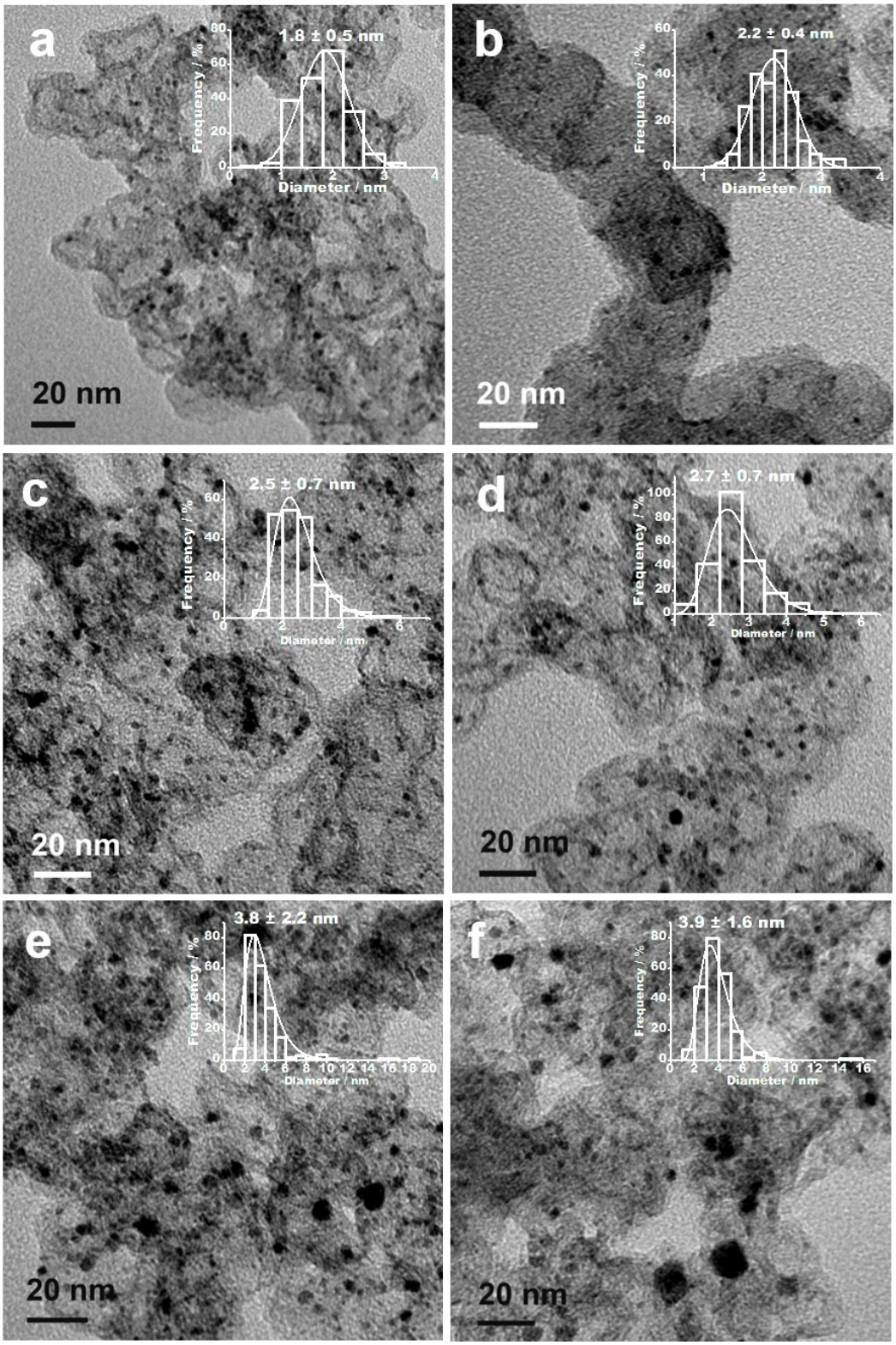

Fig. S9 TEM images of Ru/N-C synthesized at different temperature. (a) 250°C; (b) 350°C; (c) 450°C; (d) 550°C; (e) 650°C; (f) 750°C. Inset: size distribution plotted by manually measuring at least 200 individual nanoparticles.

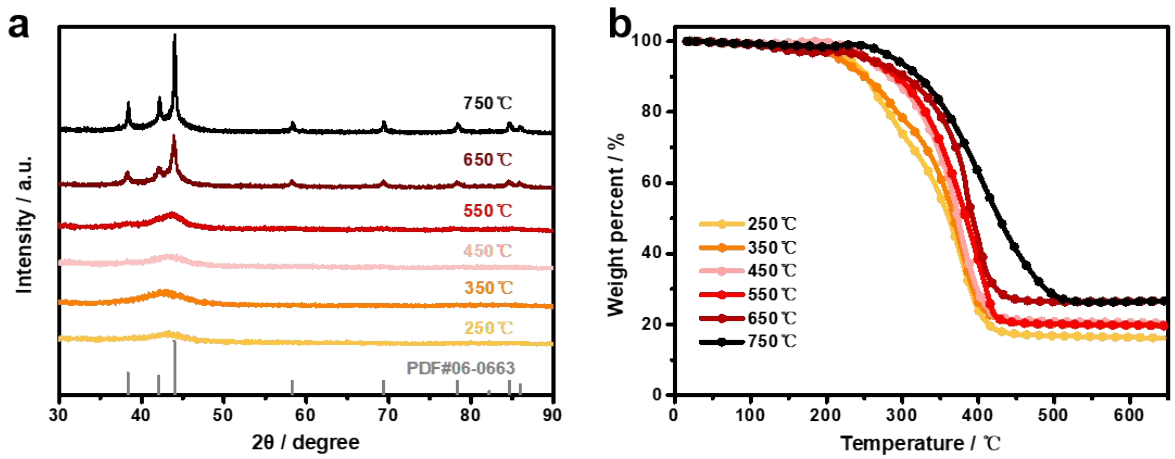

Fig. S10 (a) XRD patterns of a series of Ru/N-C obtained at different temperatures; (b) TGA curves of a series of Ru/N-C obtained at different temperatures.

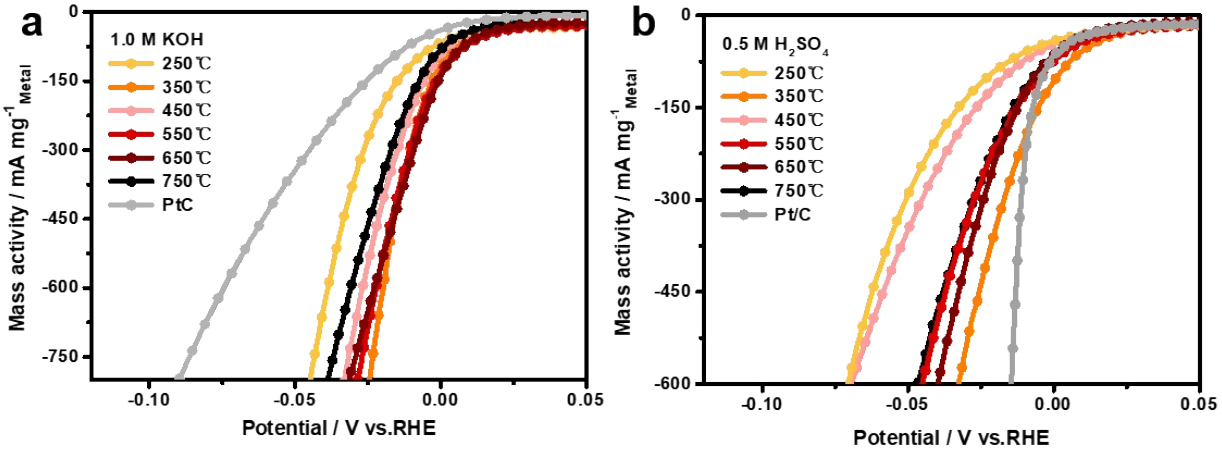

Fig. S11 Mass-normalized HER polarization curves of a series of Ru/N-C synthesized at different temperatures in 1.0 M KOH (a) and 0.5 M H_2SO_4 aqueous solution (b).

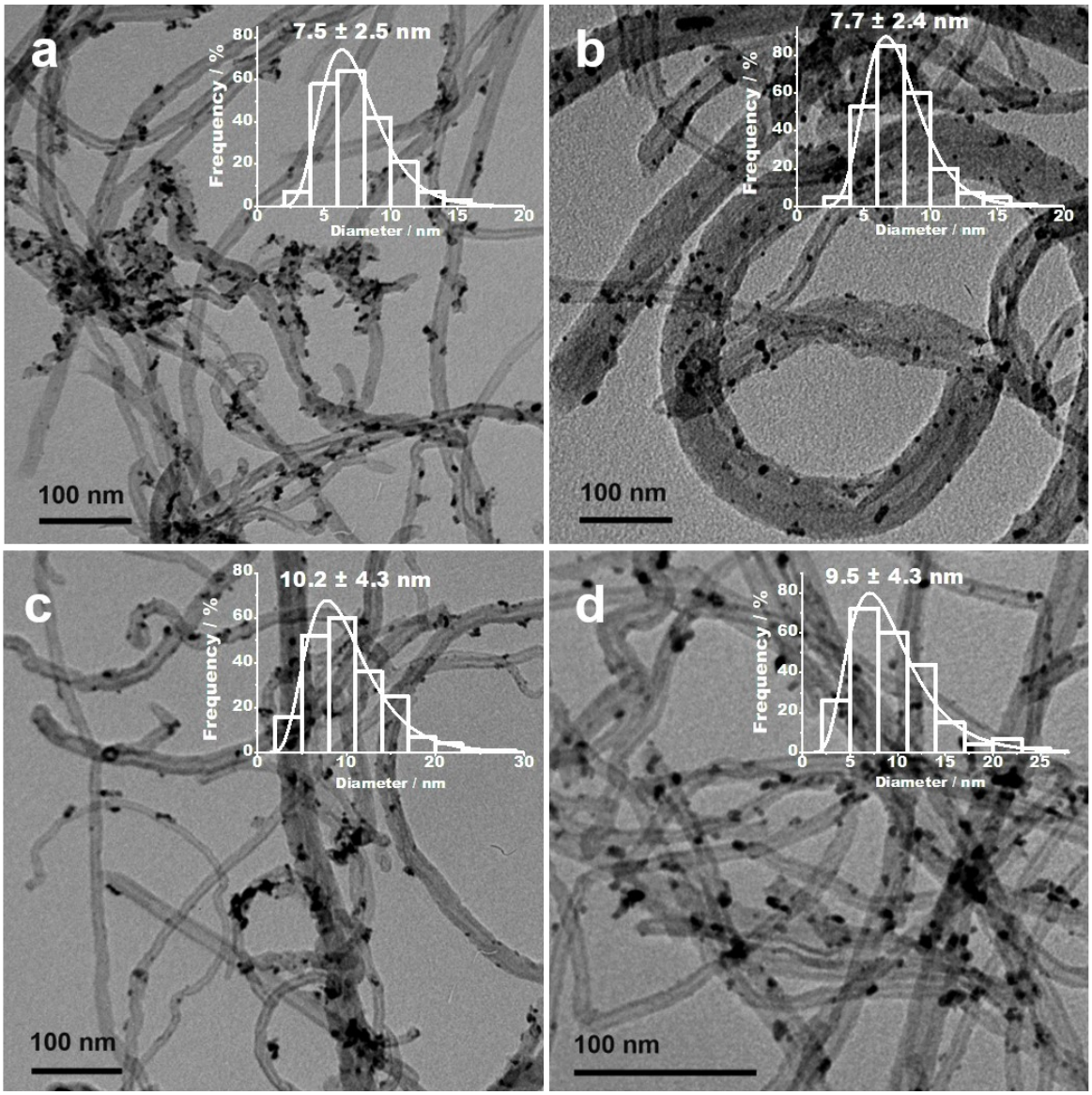

Fig. S12 TEM images of Ru NPs loaded on different N doped carriers. (a) short carboxyl multi-walled carbon nanotubes (Short MWCNT-COOH); (b) short hydroxyl multi-walled carbon nanotubes(Short MWCNT-OH); (c) hydroxyl multi-walled carbon nanotubes(MWCNT-OH); (d) multi-walled carbon nanotubes (MWCNT). Inset: size distribution plotted by manually measuring at least 200 individual nanoparticles.

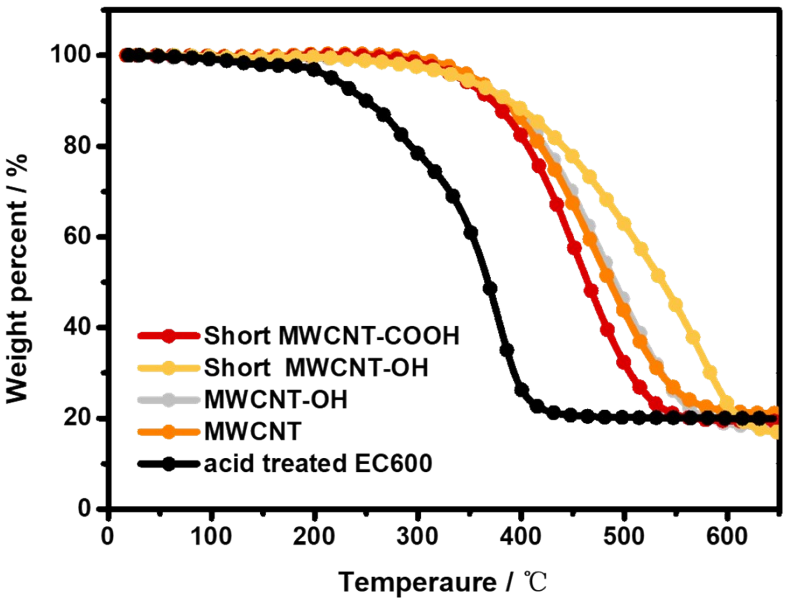

Fig. S13 TGA curves of Ru NPs loaded on N doped different carriers.

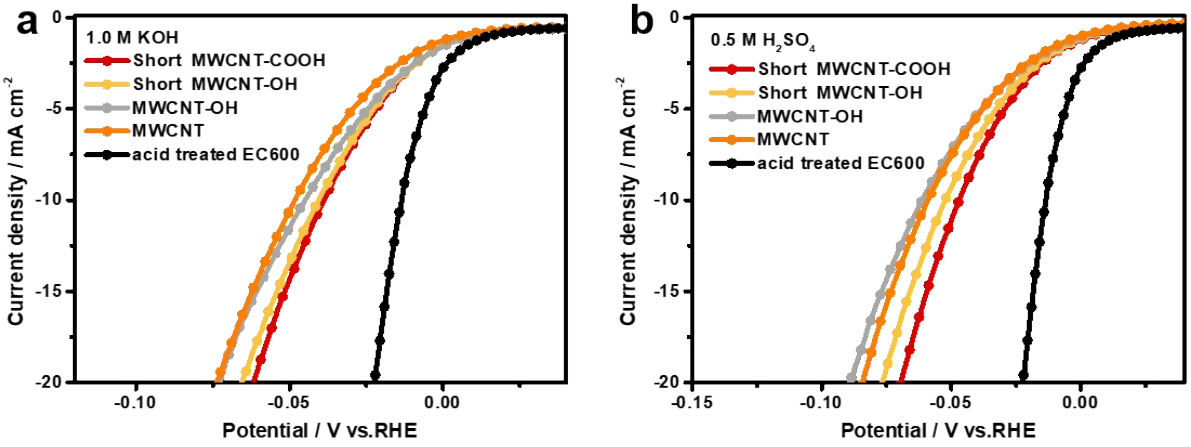

Fig. S14 HER polarization curves of Ru NPs loaded on N doped different carriers including Short MWCNT-COOH, Short MWCNT-OH, MWCNT-OH, MWCNT and EC600 in 1.0 M KOH (a) and 0.5 M H_2SO_4 (b) aqueous solution.

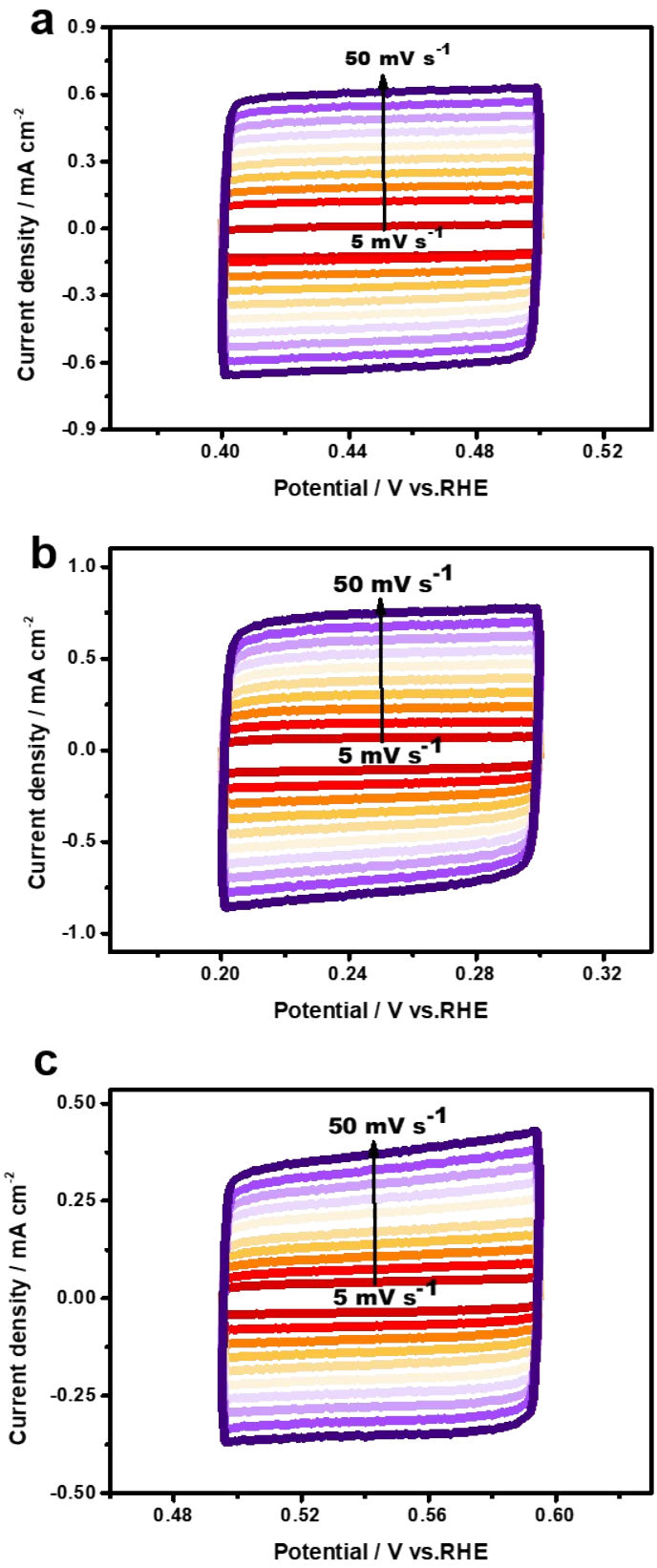

Fig. S15 CV curves measured at non-Faraday region with a scan rate from 5 to 50 mV s^{-1} for Pd/N-C (a), Ag/N-C (b), and commercial Pt/C (c).

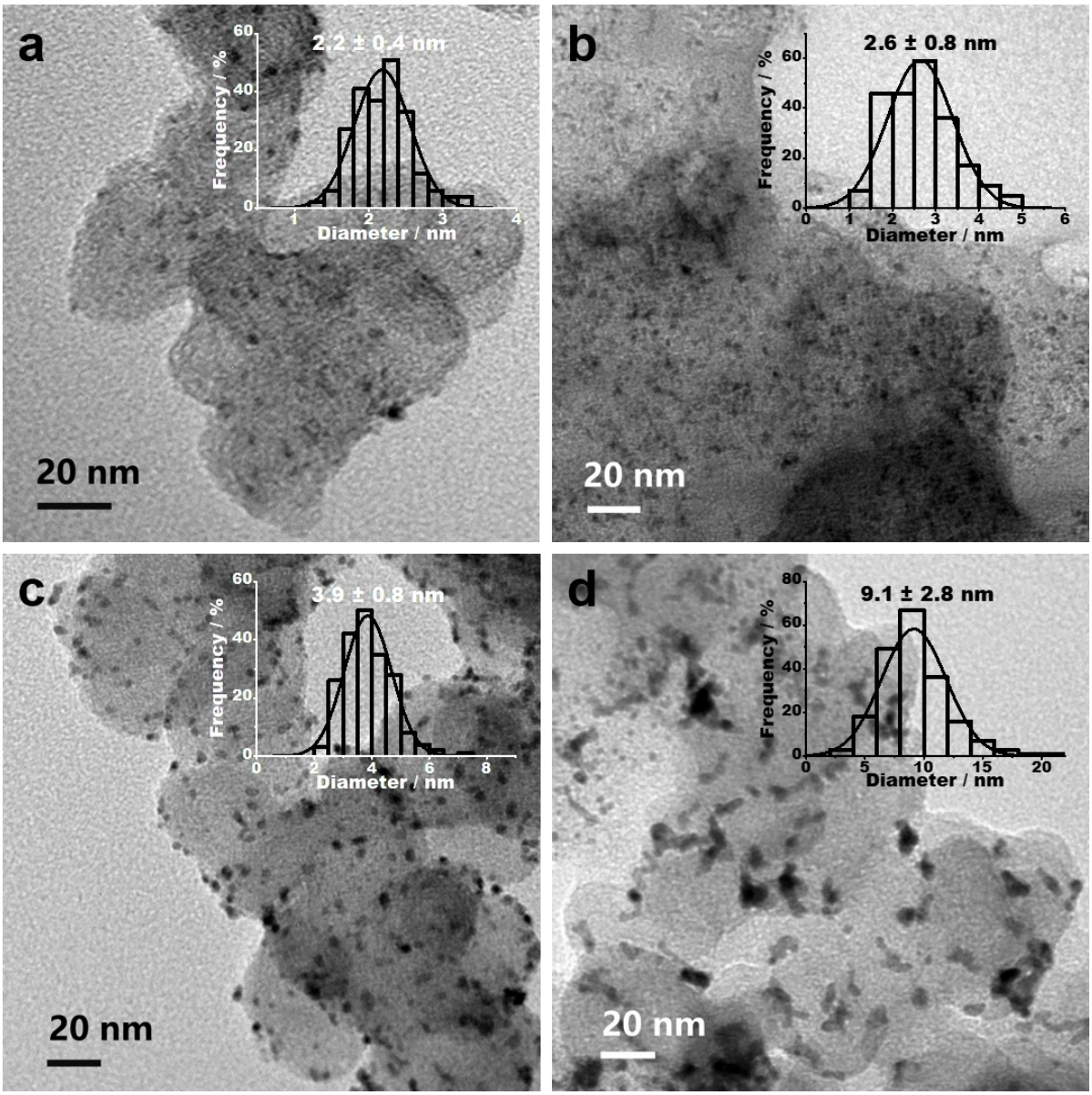

Fig. S16 TEM images of Ru/N-C initially (a) and after (b) 10000 times of potential cycles; TEM images of commercial Pt/C initially (c) and after (d) 10000 times of potential cycles in 1.0 M KOH aqueous solution. Insets: corresponding size distribution plotted by manually measuring at least 200 individual nanoparticles.

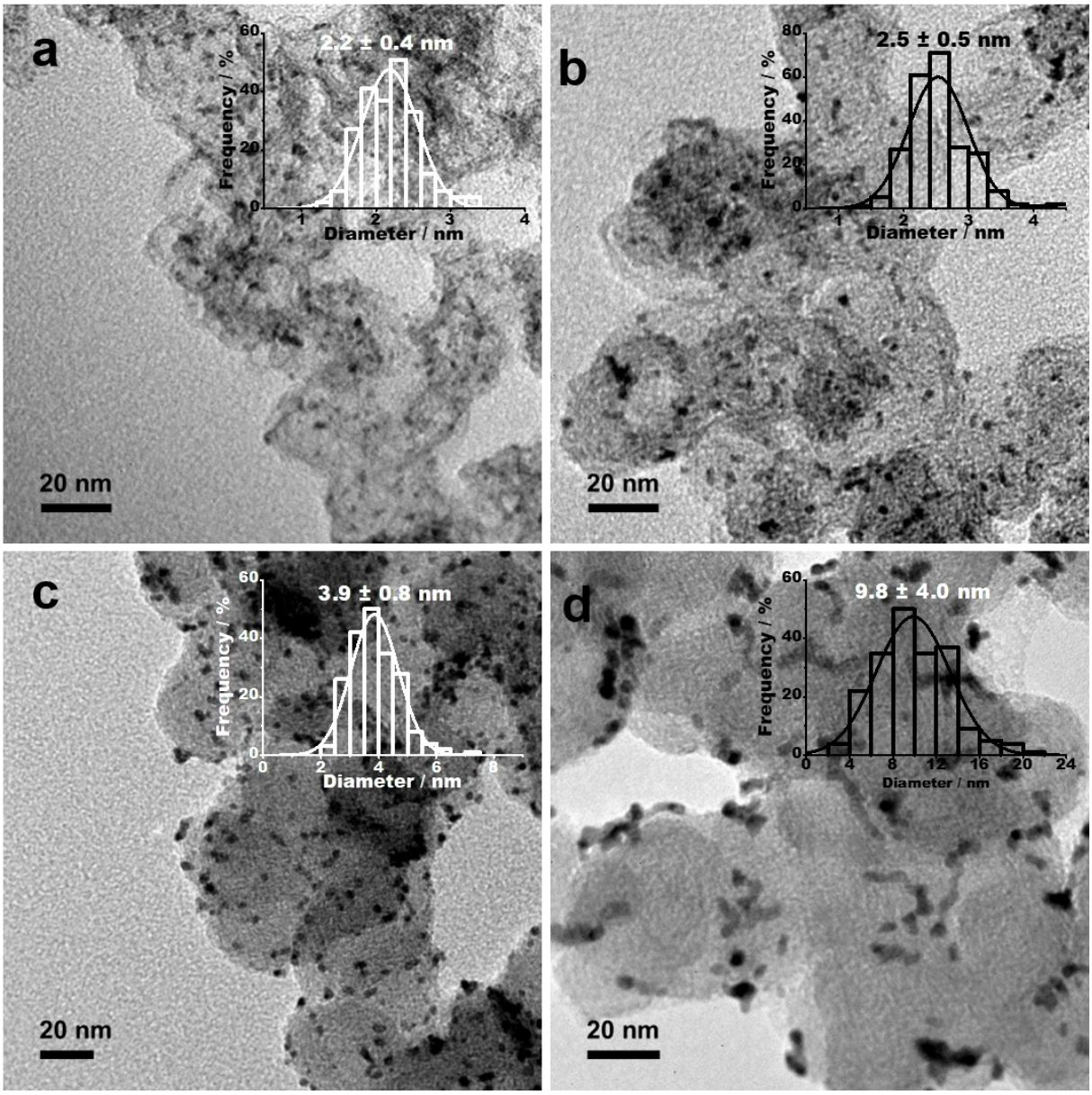

Fig. S17 TEM images of Ru/N-C before (a) and after (b) 12 h of chronopotentiometry test; TEM images of commercial Pt/C before (c) and after (d) 12 h of chronopotentiometry test at a constant cathodic current density of 10 mA cm^{-2} in 1.0 M KOH aqueous solution. Insets: corresponding size distribution plotted by measuring at least 200 individual nanoparticles.

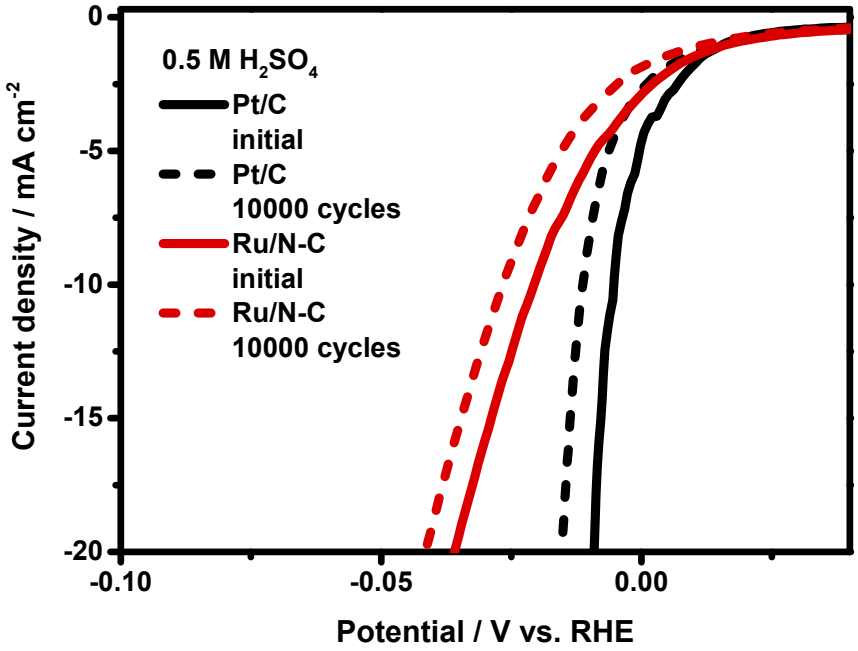

Fig. S18 HER polarization curves of Ru/N-C and commercial Pt/C before and after 10000 times of potential cycles in 0.5 M H_2SO_4 aqueous solution.

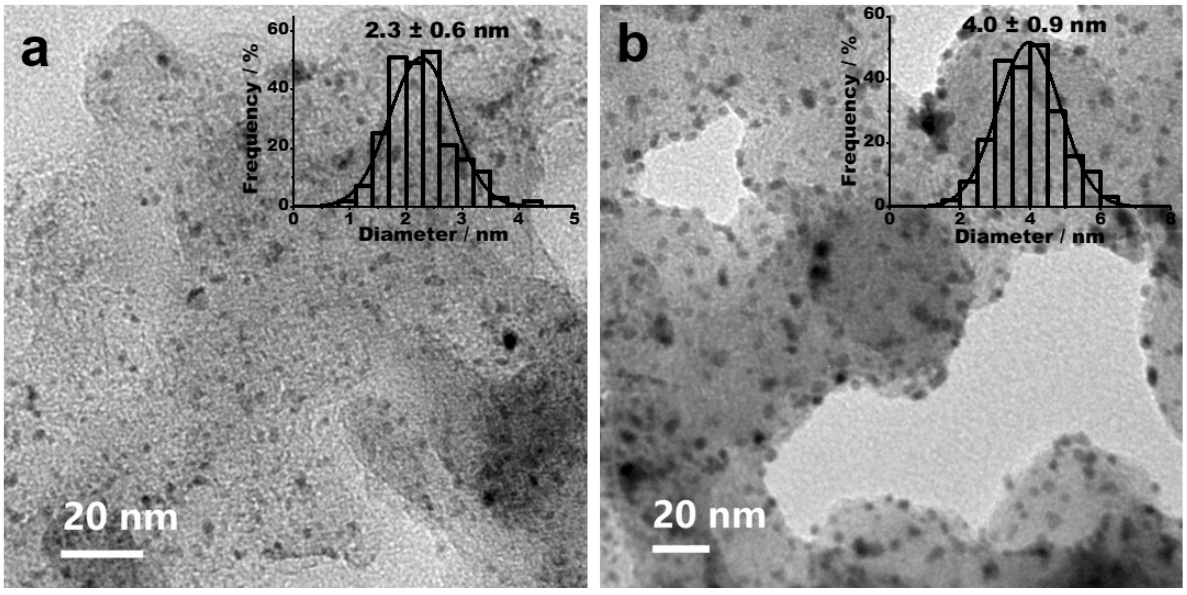

Fig. S19 TEM images of Ru/N-C (a) and commercial Pt/C (b) after 10000 times of potential cycles in 0.5 M H_2SO_4 aqueous solution. Insets: corresponding size distribution plotted by manually measuring at least 200 individual nanoparticles.

Table. S1 Elemental content of Ru/N-C according to XPS

Element	Ru	N	C	O
Atomic percent / at%	0.81	1.41	93.29	4.49

Table S2 HER activity of noble metal based electrocatalysts in acidic electrolytes

Catalyst	Catalyst Loading	Electrolyte	Overpotential (mV)	Current Density (mA cm^{-2})	Ref.
Ru/N-C	0.2 mg cm^{-2}	0.5 M H2SO4	18.5	10	This Work
RuCoP	0.3 mg cm^{-2}	0.5 M H_2SO_4	11	10	2
Ru@MWCNT	0.7 mg cm^{-2}	0.5 M H_2SO_4	13	10	3
Ru@C_2N	0.285 mg cm^{-2}	0.5 M H_2SO_4	13.5	10	4
Ru_2P@PNC@CC	----	0.5 M H_2SO_4	15	10	5
L-RP/C	0.464 mg cm^{-2}	0.5 M H_2SO_4	19	10	6
RuCu NSs/C	----	0.5 M H_2SO_4	19	10	7
Ru SAs/PN	1.0 mg cm^{-2}	0.5 M H_2SO_4	24	10	8
Ru@NGC	0.36 mg cm^{-2}	0.5 M H_2SO_4	25	10	9
RuNC	0.25 mg cm^{-2}	0.5 M H2SO4	29	10	10
RuSx/S-GO	1 mg cm^{-2}	0.5 M H_2SO_4	31	10	11
CoRu@NC	0.273 mg cm^{-2}	0.5 M H_2SO_4	32	10	12
Ag	0.2 mg cm^{-2}	0.5 M H_2SO_4	32	10	13
Ru@GLC	0.4 mg cm^{-2}	0.5 M H_2SO_4	35	10	14
RuP_2@NPC	1 mg cm^{-2}	0.5 M H_2SO_4	38	10	15
Ru0/CeO_2	0.197 mg cm^{-2}	0.5 M H_2SO_4	41	10	16
Ni-MOF@Pt	0.2 mg cm^{-2}	0.5 M H_2SO_4	43	10	17
RuP-475	0.345 mg cm^{-2}	0.5 M H_2SO_4	46	10	18
Ru-CoP/CDs	0.42 mg cm^{-2}	0.5 M H_2SO_4	49	10	19
RuCo@CDs	0.905 mg·cm^{-2}	0.5 M H_2SO_4	51	10	20
Ru@NG	0.283 mg·cm^{-2}	0.5 M H_2SO_4	53	10	21
Ru-MoO_2	0.285 mg·cm^{-2}	0.5 M H_2SO_4	55	10	22
N-RuP/NPC	0.4 mg·cm^{-2}	0.5 M H_2SO_4	58.9	10	23
RuNC-2	0.86 mg·cm^{-2}	0.5 M H_2SO_4	61	10	24
Ru-HPC	0.2 mg·cm^{-2}	0.5 M H_2SO_4	61.6	10	25
RuFeP/NC	0.36 mg·cm^{-2}	0.5 M H_2SO_4	65.8	10	26
Rh-MoS_2	0.5 mg·cm^{-2}	0.5 M H_2SO_4	67	10	27
W+RuC+BP	0.31 mg·cm^{-2}	0.5 M H_2SO_4	80	10	28
Ru-MeOH-THF	0.35 mg·cm^{-2}	0.5 M H_2SO_4	83	10	29
RuO_2-NWs@g-CN	0.214 mg·cm^{-2}	0.5 M H_2SO_4	93	10	30
RuP_2@NC	0.796 mg·cm^{-2}	0.5 M H_2SO_4	99	10	31
AgBr800	----	0.5 M H_2SO_4	108	10	32
Au/Ag HPNSs	0.212 mg cm^{-2}	0.5 M H_2SO_4	108	10	33
RuP2-550	0.345 mg cm^{-2}	0.5 M H_2SO_4	122	10	18
Ru-$MoSe_2$	0.53 mg·cm^{-2}	0.5 M H_2SO_4	143	10	34
Pd@CWN	3.8942 mg·cm^{-2}	0.5 M H_2SO_4	154	10	35
Ru-Si nanowires	0.257 mg·cm^{-2}	0.5 M H_2SO_4	200	10	36

Table S3 HER activity of noble metal based electrocatalysts in alkaline electrolytes

Catalyst	Catalyst Loading	Electrolyte	Overpotential (mV)	Current Density (mA cm^{-2})	Ref.
Ru/N-C	0.2 mg·cm^{-2}	1 M KOH	13.5	10	This Work
Ru@NG	0.857 mg cm^{-2}	1 M KOH	8	10	37
RuCo@CDs	0.905 mg·cm^{-2}	1 M KOH	11	10	20
RuNi	----	1 M KOH	15	10	38
Ru@C_2N	0.285 mg cm^{-2}	1 M KOH	17	10	4
Ru@WMCNT	0.7 mg cm^{-2}	1 M KOH	17	10	3
L-RP/C	0.464 mg cm^{-2}	1 M KOH	18	10	6
RuP-475	0.345 mg cm^{-2}	1 M KOH	22	10	18
Ru-HPC	0.2 mg·cm^{-2}	1 M KOH	22.7	10	25
RuCoP	0.3 mg cm^{-2}	1 M KOH	23	10	2
RuCo@NC	0.275 mg cm^{-2}	1 M KOH	28	10	39
Ru-MoO_2	0.285 mg cm^{-2}	1 M KOH	29	10	40
RuCu NSs/C	----	1 M KOH	29	10	7
Ru2P-BM-C	0.34 mg cm^{-2}	1 M KOH	36	10	41
RuNC-3	0.7 mg cm^{-2}	1 M KOH	38	10	42
RuNi NSs@C	3 mg cm^{-2}	1 M KOH	40	10	43
$Ni_{43}Ru_{57}$	0.28 mg cm^{-2}	1 M KOH	41	10	44
$Ru_{0.33}Se@MoS_2$	1 mg cm^{-2}	1 M KOH	45	10	45
CoRu@NC	0.273 mg cm^{-2}	1 M KOH	45	10	12
Ru2P@PNC@CC	----	1 M KOH	50	10	46
Ru-CoP/CDs	0.42 mg cm^{-2}	1 M KOH	51	10	19
RuP_2@NPC	1 mg cm^{-2}	1 M KOH	52	10	15
CoRu@MoS_2	0.390 mg cm^{-2}	1 M KOH	52	10	47
Ni_5P_4-Ru	0.142 mg cm^{-2}	1 M KOH	54	10	48
Ru-CoO	0.2 mg cm^{-2}	1 M KOH	55	10	49
Ru/rGO-V	0.204 mg cm^{-2}	1 M KOH	59.7	10	50
Rh-Rh_2O_3	----	1 M KOH	63	10	51
8.3%Rh-MoSe	0.5 mg cm^{-2}	1 M KOH	73	10	52
SARu-MoS_2	0.285 mg·cm^{-2}	1 M KOH	76	10	53
RuNC-2	0.86 mg·cm^{-2}	1 M KOH	81	10	24
Ag-Ni_3S_2	----	1 M KOH	89	10	54
S-RuP@NPSC	0.357 mg·cm^{-2}	1 M KOH	92	10	55
RuO_2-NWs@g-CN	0.214 mg·cm^{-2}	1 M KOH	95	10	30
RuP_2@NC	0.796 mg·cm^{-2}	1 M KOH	98	10	31
Ni-MOF@Pt	0.2 mg cm^{-2}	1 M KOH	102	10	17
Ag@NC	14.15 mg cm^{-2}	1 M KOH	189	10	56

Table. S4 Surface area of different commercial carbon supports (From product manufacturer data)

Carbon support	short hydroxyl multi-walled carbon nanotubes	short carboxyl multi-walled carbon nanotubes	hydroxyl multi-walled carbon nanotubes	multi-walled carbon nanotubes	EC600
Specific Surface Area / $m^2 g^{-1}$	>170	>160	>233	>140	1270

References:

1. I. A. Safo, M. Werheid, C. Dosche and M. Oezaslan, Chem. Commun., 2019, 1, 3095.
2. J. Xu, T. Liu, J. Li, B. Li, Y. Liu, B. Zhang, D. Xiong, I. Amorim, W. Li and L. Liu, Energy Environ. Sci., 2018, 11, 1819-1827.
3. D. H. Kweon, M. S. Okyay, S. Kim, J. Jeon, H. Noh, N. Park, J. Mahmood and J. Baek, Nat. Commun., 2020, 11.
4. J. Mahmood, F. Li, S. Jung, M. S. Okyay, I. Ahmad, S. Kim, N. Park, H. Y. Jeong and J. Baek, Nat. Nanotechnol., 2017, 12, 441-446.
5. T. Liu, B. Feng, X. Wu, Y. Niu, W. Hu and C. M. Li, ACS Appl. Energy Mater., 2018, 1, 3143-3150.
6. J. Yu, Y. Guo, S. She, S. Miao, M. Ni, W. Zhou, M. Liu and Z. Shao, Adv. Mater., 2018, 30, 1800047.
7. Q. Yao, B. Huang, N. Zhang, M. Sun, Q. Shao and X. Huang, Angew. Chem., Int. Ed., 2019, 58, 13983-13988.
8. J. Yang, B. Chen, X. Liu, W. Liu, Z. Li, J. Dong, W. Chen, W. Yan, T. Yao, X. Duan, Y. Wu and Y. Li, Angew. Chem., Int. Ed, 2018, 57, 9495-9500.
9. Q. Song, X. Qiao, L. Liu, Z. Xue, C. Huang and T. Wang, Chem. Commun., 2019, 55, 965-968.
10. B. Lu, L. Guo, F. Wu, Y. Peng, J. E. Lu, T. J. Smart, N. Wang, Y. Z. Finfrock, D. Morris, P. Zhang, N. Li, P. Gao, Y. Ping and S. Chen, Nat. Commun., 2019, 10.
11. P. Li, X. Duan, S. Wang, L. Zheng, Y. Li, H. Duan, Y. Kuang and X. Sun, Small, 2019, 15, 1904043.
12. Y. Xu, Y. Li, S. Yin, H. Yu, H. Xue, X. Li, H. Wang and L. Wang, Nanotechnology, 2018, 29, 225403.
13. Z. Li, J. Fu, Y. Feng, C. Dong, H. Liu and X. Du, Nat. Catal., 2019, 2, 1107-1114.
14. Z. Chen, J. Lu, Y. Ai, Y. Ji, T. Adschiri and L. Wan, ACS Appl. Mater. Inter., 2016, 8, 35132-35137.
15. Z. Pu, I. S. Amiinu, Z. Kou, W. Li and S. Mu, Angew. Chem., Int. Ed., 2017, 56, 11559-11564.
16. E. Demir, S. Akbayrak, A. M. Önal and S. Özkar, ACS Appl. Mater. Interfaces, 2018, 10, 6299-6308.
17. K. Rui, G. Zhao, M. Lao, P. Cui, X. Zheng, X. Zheng, J. Zhu, W. Huang, S. X. Dou and W. Sun, Nano Lett., 2019, 19, 8447-8453.
18. Q. Chang, J. Ma, Y. Zhu, Z. Li, D. Xu, X. Duan, W. Peng, Y. Li, G. Zhang, F. Zhang and X. Fan, ACS Sustain. Chem. Eng., 2018, 6, 6388-6394.
19. H. Song, M. Wu, Z. Tang, J. S. Tse, B. Yang and S. Lu, Angew. Chem., Int. Ed., 2021, 60, 7234-7244.
20. T. Feng, G. Yu, S. Tao, S. Zhu, R. Ku, R. Zhang, Q. Zeng, M. Yang, Y. Chen, W. Chen, W. Chen and B. Yang,

J. Mater. Chem. A, 2020, 8, 9638-9645.
21. R. Ye, Y. Liu, Z. Peng, T. Wang, A. S. Jalilov, B. I. Yakobson, S. Wei and J. M. Tour, ACS Appl. Mater. Interfaces, 2017, 9, 3785-3791.
22. P. Jiang, Y. Yang, R. Shi, G. Xia, J. Chen, J. Su and Q. Chen, J. Mater. Chem. A, 2017, 5, 5475-5485.
23. J. Zhu, S. Li, M. Xiao, X. Zhao, G. Li, Z. Bai, M. Li, Y. Hu, R. Feng, W. Liu, R. Gao, D. Su, A. Yu and Z. Chen, Nano Energy, 2020, 77, 105212.
24. Y. Li, F. Chu, Y. Liu, Y. Kong, Y. Tao, Y. Li and Y. Qin, Chem. Commun., 2018, 54, 13076-13079.
25. T. Qiu, Z. Liang, W. Guo, S. Gao, C. Qu, H. Tabassum, H. Zhang, B. Zhu, R. Zou and Y. Shao-Horn, Nano Energy, 2019, 58, 1-10.
26. B. Yang, J. Xu, D. Bin, J. Wang, J. Zhao, Y. Liu, B. Li, X. Fang, Y. Liu, L. Qiao, L. Liu and B. Liu, Appl. Catal. B, 2021, 283, 119583.
27. X. Meng, C. Ma, L. Jiang, R. Si, X. Meng, Y. Tu, L. Yu, X. Bao and D. Deng, Angew. Chem., Int. Ed., 2020, 59, 10502-10507.
28. U. Joshi, S. Malkhandi, Y. Ren, T. L. Tan, S. Y. Chiam and B. S. Yeo, ACS Appl. Mater. Interfaces, 2018, 10, 6354-6360.
29. S. Drouet, J. Creus, V. Collière, C. Amiens, J. García-Antón, X. Sala and K. Philippot, Chem. Commun., 2017, 53, 11713-11716.
30. T. Bhowmik, M. K. Kundu and S. Barman, ACS Appl. Mater. Interfaces, 2016, 8, 28678-28688.
31. B. Guo, X. Zhang, J. Xie, Y. Shan, R. Fan, W. Yu, M. Li, D. Liu, Y. Chai and B. Dong, Int. J. Hydrog. Energy, 2021, 46, 7964-7973.
32. J. Huang and Y. Wu, ACS Sustain. Chem. Eng., 2018, 6, 8285-8290.
33. Z. Zhao, H. Wu and C. Li, Energy, 2021, 218, 119520.
34. K. Vasu, O. E. Meiron, A. N. Enyashin, R. Bar-Ziv and M. Bar-Sadan, The J. Phys. Chem. C, 2019, 123, 1987-1994.
35. W. Deng, Y. Li, F. Wang, Q. Ma and S. Min, Electrocatalysis, 2021, 12, 340-349.
36. L. Zhu, Q. Cai, F. Liao, M. Sheng, B. Wu and M. Shao, Electrochem commun, 2015, 52, 29-33.
37. B.K.Barman, D.Das and K. K.Nanda, Sustain. Energy Fuels, 2017, 1, 1028–1033
38. G. Liu, W. Zhou, B. Chen, Q. Zhang, X. Cui, B. Li, Z. Lai, Y. Chen, Z. Zhang, L. Gu and H. Zhang, Nano Energy, 2019, 66, 104173.
39. J. Su, Y. Yang, G. Xia, J. Chen, P. Jiang and Q. Chen, Nat. Commun., 2017, 8.
40. P. Jiang, Y. Yang, R. Shi, G. Xia, J. Chen, J. Su and Q. Chen, J. Mater. Chem. A, 2017, 5, 5475-5485.
41. X. Liu, Y. Guo, W. Zhan and T. Jin, Catalysts, 2019, 9, 240.
42. Y. Li, F. Chu, Y. Liu, Y. Kong, Y. Tao, Y. Li and Y. Qin, Chem. Commun., 2018, 54, 13076-13079.
43. J. Ding, Q. Shao, Y. Feng and X. Huang, Nano Energy, 2018, 47, 1-7.
44. Q. He, D. Tian, H. Jiang, D. Cao, S. Wei, D. Liu, P. Song, Y. Lin and L. Song, Adv. Mater., 2020, 32, 1906972.
45. Q. Chen, K. Wang, J. Qin, S. Wang, W. Wei, J. Wang, Q. Shen, P. Qu and D. Liu, RSC Adv., 2019, 9, 13486-13493.
46. T. Liu, B. Feng, X. Wu, Y. Niu, W. Hu and C. M. Li, ACS Appl. Energy Mater., 2018, 1, 3143-3150.
47. I. S. Kwon, T. T. Debela, I. H. Kwak, Y. C. Park, J. Seo, J. Y. Shim, S. J. Yoo, J. G. Kim, J. Park and H. S. Kang, Small, 2020, 16, 2000081.
48. Q. He, D. Tian, H. Jiang, D. Cao, S. Wei, D. Liu, P. Song, Y. Lin and L. Song, Adv. Mater, 2020, 32, 1906972.
49. J. Guo, D. Yan, K. Qiu, C. Mu, D. Jiao, J. Mao, H. Wang and T. Ling, J. Energy Chem., 2019, 37, 143-147.
50. X. Que, T. Lin, S. Li, X. Chen, C. Hu, Y. Wang, M. Shi, J. Peng, J. Li, J. Ma and M. Zhai, Appl. Surf. Sci., 2021, 541, 148345.
51. M. K. Kundu, R. Mishra, T. Bhowmik and S. Barman, J. Mater. Chem. A, 2018, 6, 23531-23541.
52. X. Meng, C. Ma, L. Jiang, R. Si, X. Meng, Y. Tu, L. Yu, X. Bao and D. Deng, Angew. Chem., Int. Ed., 2020,

59, 10502-10507.
53. J. Zhang, X. Xu, L. Yang, D. Cheng and D. Cao, Small Methods, 2019, 3, 1900653.
54. C. Liu, F. Wang, D. Jia, J. Zhang, J. Zhang, Q. Hao, J. Zhang, Y. Li and H. Liu, Nanoscale, 2020, 12, 19333-19339.
55. X. Liu, F. Liu, J. Yu, G. Xiong, L. Zhao, Y. Sang, S. Zuo, J. Zhang, H. Liu and W. Zhou, Adv. Sci., 2020, 7, 2001526.
56. X. Liang and Y. Li, J. Porous Mater., 2020, 27, 1213-1218.